Tannin-based biosorbent encapsulated into calcium alginate beads for Cr(VI) removal

Xubing Sun, Jiayong Zhang, Guowen Ding and Yaohui You

ABSTRACT

A composite biosorbent (AC-TFR) prepared by encapsulating tannin-formaldehyde resin (TFR) into calcium alginate (AC) beads was used to remove Cr(VI) from an aqueous solution. Various influencing factors, such as TFR dosage, pH, initial Cr(VI) concentration, contact time, temperature and presence of co-ions in the medium, were investigated. The structures and adsorption performances of the adsorbents were characterized by Fourier transform infrared spectroscopy (FTIR), scanning electron microscopy (SEM), X-ray diffraction (XRD) and X-ray photoelectron spectroscopy (XPS). Compared with other AC-TFR adsorbents, AC-TFR-2 (mass ratio of AC:TFR = 1:1) showed an excellent adsorption capacity based on the efficiency of Cr(VI) removal. The kinetic data fitted to pseudo-second-order and intra-particle diffusion models suggested that the adsorption process was subject to a rate-controlling step. The equilibrium adsorption data fitted well to the Langmuir isotherm model, and the maximum adsorption capacities of AC-TFR-2 were 145.99, 167.22 and 174.52 mg/g at 288, 298, and 308 K, respectively. The thermodynamic parameters revealed that Cr(VI) removal by AC-TFR-2 was endothermic and spontaneous, and the process was chemical adsorption. The mechanism of Cr(VI) removal consisted first of reduction to Cr(III), which has a low toxicity, and then chelation onto AC-TFR-2 via ion exchange.

Key words | adsorption, calcium alginate, Cr(VI), tannin-formaldehyde resin

Xubing Sun (corresponding author)
Yaohui You
Key Laboratory of Fruit Waste Treatment and Resource Recycling of the Sichuan Provincial Higher Learning Institutes,
Neijiang, Sichuan Province 641100,
China
E-mail: *njtcsunxb@163.com*

Xubing Sun
Jiayong Zhang
Guowen Ding
Yaohui You
College of Chemistry and Chemical Engineering,
Neijiang Normal University,
Neijiang, Sichuan Province 641100,
China

INTRODUCTION

With the rapid development of industry, potentially toxic metals have been extremely important in scientific and technological terms and have therefore been widely used. The subsequent potentially toxic metal pollution, threatens the sustainable development of the environment and human health. Among the potentially toxic metals, chromium (Cr) is a common pollutant that is widely used in electroplating, leather tanning, metal finishing, photography, and nuclear power plants (Aharchaou *et al.* 2018). In the environment, Cr occurs mainly in two stable oxidation forms, trivalent (Cr(III), positively charged at acidic pH) and hexavalent (Cr(VI), negatively charged), and these have different toxicities (Sillerová *et al.* 2015). Cr(III) is recognized as an essential element for human health at low concentrations and is less toxic, whereas Cr(VI) has a toxicity that is 500 times higher than that of Cr(III) (Chand *et al.* 2009). Repeated exposure to Cr(III) causes non-lethal health effects, while exposure to Cr(VI) may lead to respiratory disease, fibrosis, perforation of the nasal septum, development of nasal polyps and lung carcinoma (Kumar *et al.* 2013). The maximum concentrations of Cr(VI) discharged into inland surface and drinking waters are legally limited to 0.1 mg/L and 0.05 mg/L, respectively (Kumar *et al.* 2017). Therefore, it is necessary to manage water and industrial contaminants containing Cr(VI) to decrease the Cr(VI) concentrations to within the permitted limits before discharge into the environment.

At present, many technologies are applied to minimize Cr(VI) discharge, such as chemical precipitation, ion exchange, filtration, solvent extraction, membrane separation, chemical coagulation, adsorption, etc (Wang *et al.* 2016; Habiba *et al.* 2017a, 2017b). In general, adsorption is a widely used technology for Cr(VI) removal due to its efficiency, adaptability, lower sludge production and economical practicability (Gopalakannan & Viswanathan 2016; Liu *et al.* 2018). According to studies in the literature, various sorbents have been employed for Cr(VI) removal, such as grape waste (Chand *et al.* 2009), carbon nanotubes

doi: 10.2166/wst.2020.178

(Ren *et al.* 2011), bentonite (Zhao *et al.* 2015), graphene oxide (Wang *et al.* 2017), hydroxyapatite (Hokkanen *et al.* 2016; Doan *et al.* 2019), active carbon (Suganya & Kumar 2018), etc.

Tannin-formaldehyde resin (TFR), containing o-dihydroxy and trihydroxy aromatic rings, is capable of forming chelates with metal ions (positively charged) and has been widely applied in wastewater treatment for potentially toxic metal removal (Arbenz & Avérous 2015; Bacelo *et al.* 2016). Moreover, TFR is also applied in Cr(VI) removal due to the strong reducibility of the hydroxylphenyl groups which can reduce Cr(VI) to Cr(III) (Bacelo *et al.* 2016). From an environmental point of view, it is beneficial. Despite being a good adsorbent, there are a few challenging issues with TFR, such as the small particle size, low density and poor recovery, which hamper its practical applications (Kumar *et al.* 2017; Nasrullah *et al.* 2017). To reduce the limitations, TFR might be encapsulated in a polymeric matrix. The encapsulation could facilitate recovery of the exhausted composite adsorbent. Calcium alginate (AC) has been used extensively as an encapsulation gel material because the technique is simple, biocompatible, and low cost (Fiol *et al.* 2005). AC itself shows electrostatic attraction to potentially toxic metal ions (positively charged) by the negatively charged carboxyl groups on the AC surface (Ibáñez & Umetsu 2002; Googerdchian *et al.* 2012). But it exhibits no attraction towards Cr(VI) (negatively charged) (Xu *et al.* 2013). Many studies have provided evidence that the adsorption capacity of AC for Cr(VI) is increased by immobilizing the beads with iron sulfide nanoparticles (Wu *et al.* 2017), layered double hydroxide (Lee *et al.* 2013), tannic acid-grafted-polyethyleneimine (Bertagnolli *et al.* 2015), magnetic graphene oxide (Vu *et al.* 2017), grape stalk waste (Fiol *et al.* 2005), zirconium oxide (Kumar *et al.* 2017), and goethite (Lazaridis & Charalambous 2005). However, to the best of our knowledge, few investigations have focused on the composite of AC with TFR. This study provides the first report of the removal of Cr(VI) from aqueous solution using a composite of AC with TFR.

The objective of present study was to prepare a facile, biocompatible and low-cost composite biosorbent called AC-TFR by dropping a mixture of TFR and sodium alginate into a solution of calcium dichloride. The structure and morphology of the adsorbents were characterized by Fourier transform infrared spectroscopy (FTIR), X-ray diffraction (XRD) and scanning electron microscopy (SEM) techniques, and the adsorption performance of AC-TFR for Cr(VI) removal was evaluated by the batch process. The dynamics, isotherm, thermodynamics and mechanism of Cr(VI) removal onto AC-TFR were been investigated.

MATERIALS AND METHODS

Materials

Sodium alginate with a molecular weight of 32,000–250,000 g/mol (data provided by the manufacturer) was purchased from Shanghai Yuanye Biotechnology Co., Ltd, China. Tannin extracted from black wattle bark (condensed tannin) was kindly provided by Professor Xuepin Liao of Sichuan University, China. A 37 wt% formaldehyde solution and potassium chromate were purchased from Chengdu Kelong Chemical Reagent Co., Ltd, China. All other chemicals were of analytical grade and used as received.

Preparation of the adsorbents

Synthesis of TFR

TFR was synthesized by acid-catalysed polymerization according to a previous study (Gurung *et al.* 2011). A total of 2.0 g of black wattle tannin was dissolved in 30 mL of a 0.5 mol L^{-1} HCl solution. Afterwards, 1 mL of a 37 wt% formaldehyde solution was added and stirred at 363 K for 3 hours. Finally, a fine powder product was obtained by filtration, washing with distilled water and absolute alcohol to remove any unreacted substances and drying under vacuum at 333 K for 12 hours.

Preparation of AC-TFR

The composite AC-TFR beads were synthesized by adding a mixture of TFR and sodium alginate to a solution of calcium dichloride. First, 2.0 wt% sodium alginate was prepared by dissolving 1.0 g of sodium alginate in 50 mL of distilled water at 313 K until a homogeneous solution was obtained. Subsequently, a certain amount of TFR was added to the solution under constant stirring for 4 hours and then treated with ultrasound for 15 min. The resulting solution was carefully fed into a 2 wt% $CaCl_2$ solution through a syringe with a diameter of 0.64 mm to form beads. The beads, approximately 2.5–3 mm in diameter, were hardened for 1 hour in the $CaCl_2$ solution, washed three times with distilled water to remove any remaining $CaCl_2$ and then freeze dried for 24 hours. The beads prepared with different amounts of TFR (0, 0.5, 1, 1.5 and 2 g) were called AC, AC-TFR-1, AC-TFR-2, AC-TFR-3 and AC-TFR-4, respectively.

Characterization of the adsorbents

The surface and inner morphologies of the adsorbents were examined by SEM (TESCAN VEGA3, Czech). FTIR spectra (Thermo Fisher Scientific, USA) of the samples blended with KBr and pressed into pellets were recorded in the range of 400–4,000 cm^{-1}. XRD (DX-2700X, China) analysis was carried out to characterize the crystal structures of the samples. X-ray photoelectron spectroscopy (XPS) (XSAM-800, UK) was performed to determine the elements in the adsorbents before and after Cr(VI) adsorption. Peaks of the XPS spectra were fitted with XPSPEAK4.1 software and 20% Lorentzian-Gaussian.

Batch adsorption experiments

All batch adsorption experiments were carried out in a 250 mL conical flask with a cover by adding 0.1 g of AC-TFR to 100 mL of a Cr(VI) solution under shaking at a speed of 200 rpm in a constant-temperature shaker (Guohua, SHA-C, China). Different parameters of Cr(VI) removal were examined, including the effect of the pH (2–10), mass of TFR (0.5–2 g), contact time (0–24 hours), initial concentration of Cr(VI) (25–500 mg/L) and temperature (288–308 K). The Cr(VI) concentration in the supernatant was determined using the 1,5-diphenyl carbazide method at a wavelength of 540 nm with a UV-vis spectrophotometer (Persee, TU-1950, China) (Han *et al.* 2016). Solutions with concentrations higher than the detection limit of the spectrophotometer were diluted before analysis. All of the adsorption experiments were carried out in triplicate to obtain the average value and minimize error.

The Cr(VI) adsorption capacity at equilibrium q_e (mg/g), the Cr(VI) adsorption capacity at time t, q_t (mg/g) and the Cr(VI) removal rate (%) were calculated using Equations (1)–(3), respectively.

$$q_e = (C_0 - C_e)\frac{V}{m} \quad (1)$$

$$q_t = (C_0 - C_t)\frac{V}{m} \quad (2)$$

$$\text{Removal rate} = \frac{C_0 - C_e}{C_0} \times 100\% \quad (3)$$

where C_0 (mg/L), C_t (mg/L) and C_e (mg/L) are the concentrations of the Cr(VI) solution at the start, time t and adsorption equilibrium, respectively, V (L) is the total volume of the Cr(VI) solution and m (g) is the amount of the adsorbent.

RESULTS AND DISCUSSION

Characterization

Figure 1(a) shows the FTIR spectra of AC, TFR and AC-TFR-2 in the region of 400–4,000 cm^{-1}. In all of the spectra, the broad peak in the region of 3,600–3,100 cm^{-1} was attributed to the stretching vibration of the O–H bonds of phenolic or alcoholic groups, and the narrow peaks at approximately 2,900 cm^{-1} were related to the stretching vibration of C-H (Kamel *et al.* 2013). The peaks at 1,628.14, 1,423.74 and 1,030.38 cm^{-1} among the FTIR spectra of AC were attributed to the asymmetric and symmetric stretching of carboxylate ions and C–O, respectively

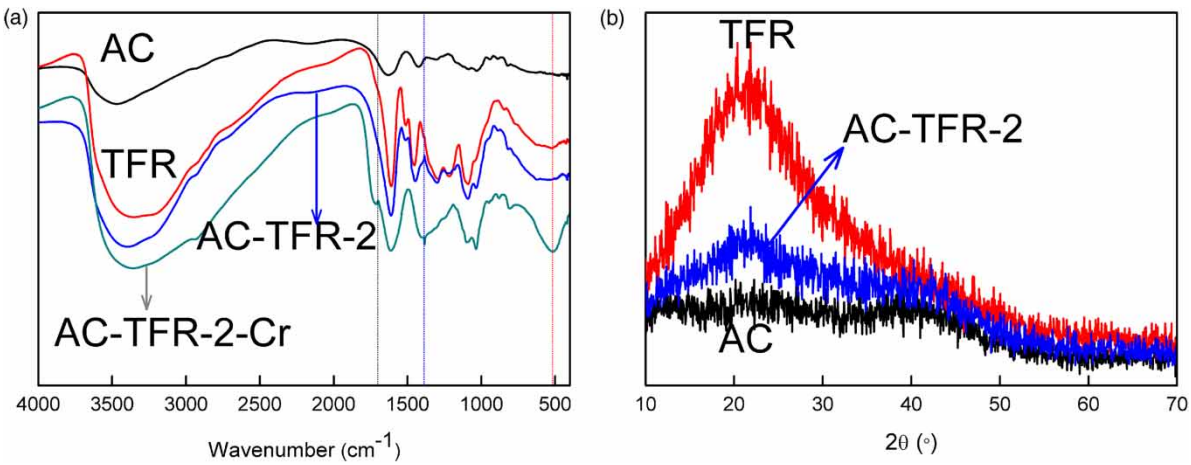

Figure 1 | (a) FTIR spectra of AC, TFR, AC-TFR-2 and AC-TFR-2-Cr; (b) XRD patterns of AC, TFR and AC-TFR-2.

(Peretz *et al.* 2015). Among the FTIR spectra of TFR, the adsorption bands at 1,609.32, 1,509.48 and 1,452.58 cm^{-1} were wide and characteristic of aromatic –C = C– bonds (Sánchez-Martín *et al.* 2010). The peaks observed at 1,293.31, 1,216.09 and 1,089 cm^{-1} were related to the C–O stretching of the aromatic rings, the methylene ether bridges formed through gelation with formaldehyde and asymmetrical C–O–C stretching, respectively (Özacar *et al.* 2008). After encapsulating TFR into AC, the peaks related to C–O at approximately 1,300.55 and 1,089.22 cm^{-1} in the spectra of AC-TFR-2 were broader than those of TFR. Another change was that the peak in the region of 3,600–3,100 cm^{-1} became narrower compared to TFR. These observations indicated the possibility of the interaction between the phenolic hydroxyl groups in TFR and calcium ions to form a coordinate structure (Şengil & Özacarb 2008).

Figure 1(b) shows the XRD patterns of AC, TFR and AC-TFR-2. Both AC and TFR showed an amorphous structure, while AC had no characteristic peak. TFR had a broad hollow peak at $2\theta = 22^{\circ}$, which represented the presence of polar functional groups (Rahman *et al.* 2014). The XRD pattern of AC-TFR-2 was superimposed onto the patterns of AC and TFR. Compared with TFR, the intensity of the peak at $2\theta = 22^{\circ}$ decreased. This result could be attributed to the formation of a chelating structure between the phenolic groups of TFR and calcium ions that induced a decrease in the polarity of the functional groups.

Figure 2 shows the morphological and surface features of AC, TFR and AC-TFR-2. The images clearly show that TFR was successfully encapsulated in AC to form AC-TFR-2 beads.

Comparison of the adsorption performances of AC-TFR

Figure 3(a) shows a comparison of the Cr(VI) adsorption capacities and removal rates of all prepared adsorbents. AC had a low adsorption capacity for Cr(VI). As TFR was encapsulated into AC, the Cr(VI) adsorption capacity and removal rate of the AC-TFR composites were greatly improved. Compared with TFR, the Cr(VI) adsorption capacity of AC-TFR decreased. It has been reported that even after the formation of AC the structure of this biopolymer leaves carboxylic groups free and the complete dissociation of the free carboxylic groups may be taking place at pH around 4.5 (Fiol *et al.* 2005). In experimental conditions, the surface of the AC-TFR beads is negatively charged and Cr(VI) exists as a series of negative ions. The electrostatic repulsion between them may explain the influence of AC in the reduction of adsorption capacity. Among all of the AC-TFR composites, AC-TFR-2 (mass ratio of AC:TFR = 1:1) had the highest adsorption capacity and removal rate under the same conditions. Therefore, the protocol of encapsulating TFR into AC improved the adsorption of AC for Cr(VI).

Influence of the pH

In an aqueous solution, Cr(VI) exists as a series of negative ions, including $HCrO_4^-$, CrO_4^{2-}, $Cr_2O_7^{2-}$ and $HCr_2O_7^{2-}$, and the distribution of these Cr(VI) species is influenced by the pH (Lazaridis & Charalambous 2005). At a pH <2, $HCrO_4^-$ is the dominant form. In the pH range of 2–6, different chromium ions, such as $HCrO_4^-$, CrO_4^{2-} and $Cr_2O_7^{2-}$, can coexist, but the main form is $HCrO_4^-$. At a pH >7.5, CrO_4^{2-} is the only chromate form (Rodrigues *et al.* 2015). Therefore, the Cr(VI) removal efficiency of AC-TFR-2 was primarily influenced by the pH of the solution.

As shown in Figure 3(b), with the increase in pH in the range of 2–10, the Cr(VI) removal rate decreased. Previous studies demonstrated that the polyhydroxyphenyl groups of TFR had a strong reducibility to Cr(VI) (Nakano *et al.* 2001; Chang *et al.* 2016). In the pH range of 2–6, Cr(VI) existing in the dominant form of $HCrO_4^-$ was reduced to the relatively friendly Cr(III) form because of its high positive potential and strong reducibility of TFR. The reaction of reducing Cr(VI) to Cr(III) can be represented as Equation (4).

$$HCrO_4^- + 7H^+ + 3e^- \rightleftharpoons Cr^{3+} + 4H_2O \quad (4)$$

The rate of the oxidation-reduction reaction was significantly influenced by the pH. At a lower pH, the reaction was more favourable (Nakajima & Baba 2004). When the adsorption process started at an initial pH of 2, the Cr(VI) removal rate was 90.54%. At a pH of 6, the Cr(VI) removal rate decreased to 24.48%. It was also observed in Figure 3(b) that the equilibrium pH of the solution changed during Cr(VI) removal via adsorption onto AC-TFR-2. In the pH range of 2–7, the equilibrium pH increased. This result was ascribed to the consumption of hydrogen ions in promoting the reduction of Cr(VI). At a pH > 7, the equilibrium pH decreased, which was deduced from the release of hydrogen ions from the polyhydroxyphenyl groups of AC-TFR-2.

Influence of the contact time and adsorption kinetics

The effect of contact time on the Cr(VI) adsorption capacity of AC-TFR-2 was examined at different times from 0 to 1,440 min, and the result is shown in Figure 3(c). It can be seen that there was a quick increase in Cr(VI) uptake

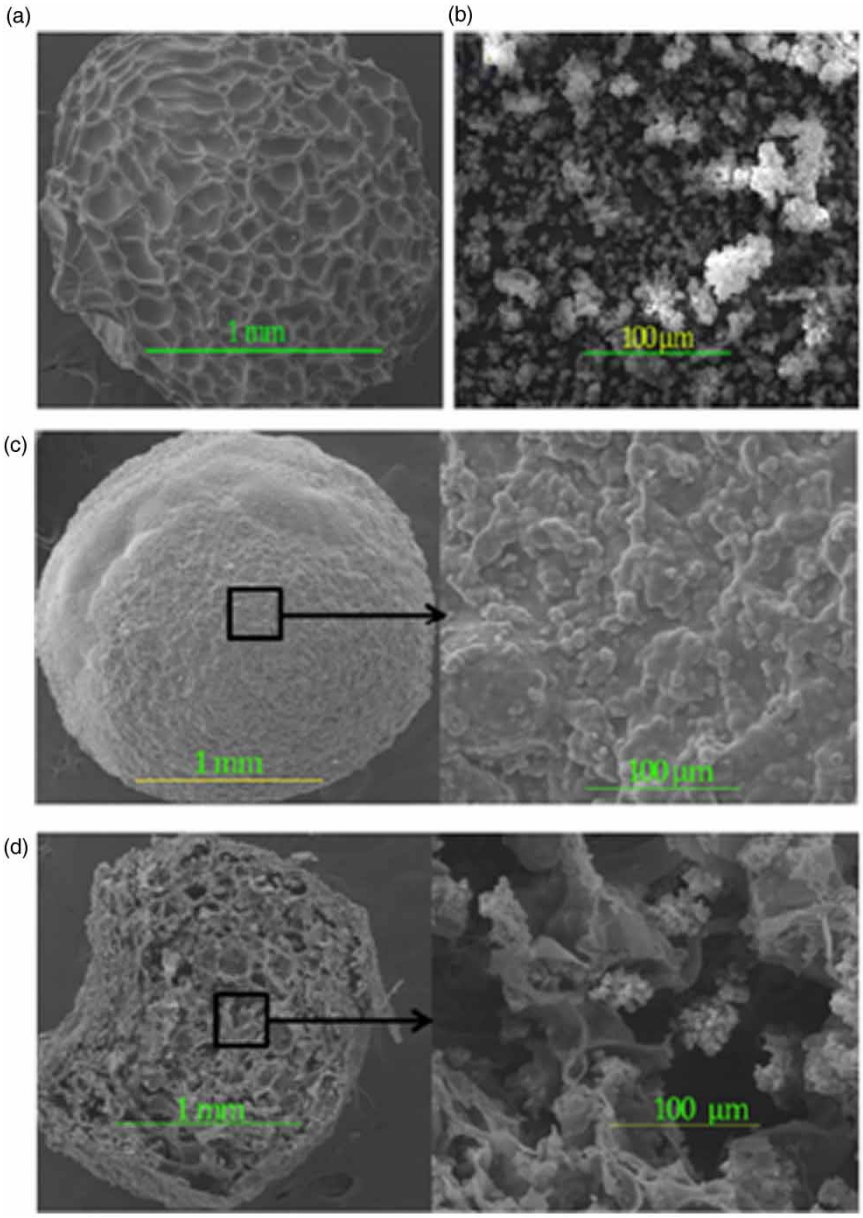

Figure 2 | SEM images of (a) AC, (b) TFR, (c) outer surface and (d) cross-section of AC-TFR-2.

during the initial 300 min. Afterwards, the adsorption process showed a low rate of increase and reached equilibrium after 1,320 min. The adsorption capacity of AC-TFR-2 after 1,440 min was 167.49 mg/g.

Pseudo-first-order (Equation (5)) and pseudo-second-order (Equation (6)) kinetic models were employed to fit the experimental data (Kumar *et al.* 2017).

$$\ln(q_e - q) = \ln q_e - k_1 t \tag{5}$$

$$\frac{t}{q_t} = \frac{1}{k_2 q_e^2} + \frac{t}{q_t} \tag{6}$$

where q_e and q_t (mg/g) are the amounts of Cr(VI) removed at equilibrium and at time t (min), respectively, k_1 (min^{-1}) is the pseudo-first-order rate constant obtained by calculating the slope of the linear equation of the $\ln(q_e - q)$ versus t plot, and k_2 (g/mg·min) is the pseudo-second-order rate constant obtained by calculating the slope of the linear equation of the t/q_t versus t plot.

The graphic fitting results of the pseudo-first-order and pseudo-second-order equations are shown in Figure 4(a). In view of the good correlation coefficient (R^2), the pseudo-second-order equation ($R^2 = 0.995$) better described

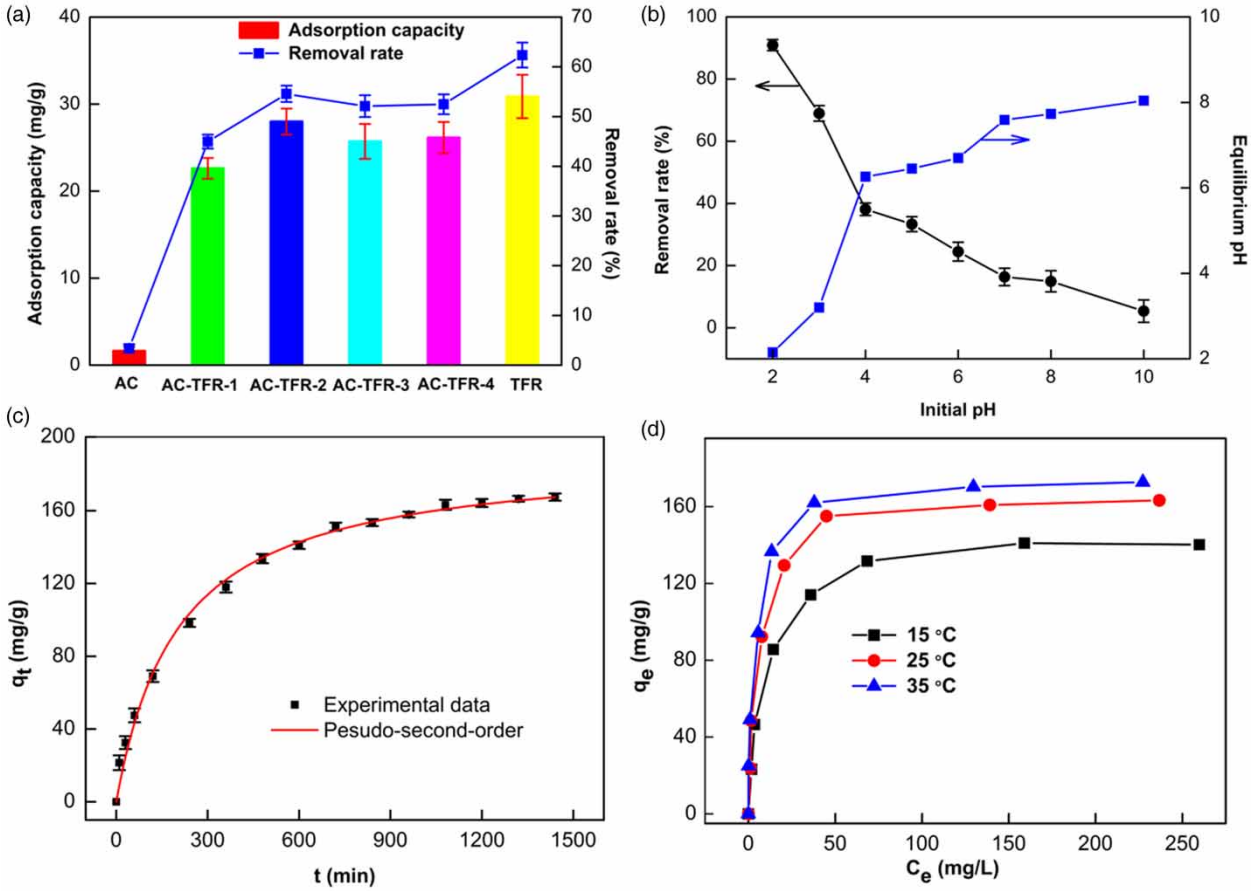

Figure 3 | (a) Cr(VI) adsorption capacity and removal rate of AC, AC-TFR-1 to AC-TFR-4 and TFR (pH = 6.33, C_0 = 50 mg/L, V = 100 mL, dosage = 0.1 g, t = 24 hours, and T = 298 K); (b) effect of the initial pH on the Cr(VI) removal rate (C_0 = 200 mg/L, V = 100 mL, dosage = 0.1 g, t = 24 hours, and T = 298 K); (c) effect of the contact time on the adsorption capacity of AC-TFR-2 for Cr(VI) (pH = 2, C_0 = 200 mg/L, V = 100 mL, dosage = 0.1 g, and T = 298 K); (d) effect of the initial concentration of Cr(VI) and temperature on the adsorption capacity of AC-TFR-2 for Cr(VI) (pH = 2, V = 100 mL, dosage = 0.1 g, and t = 24 hours).

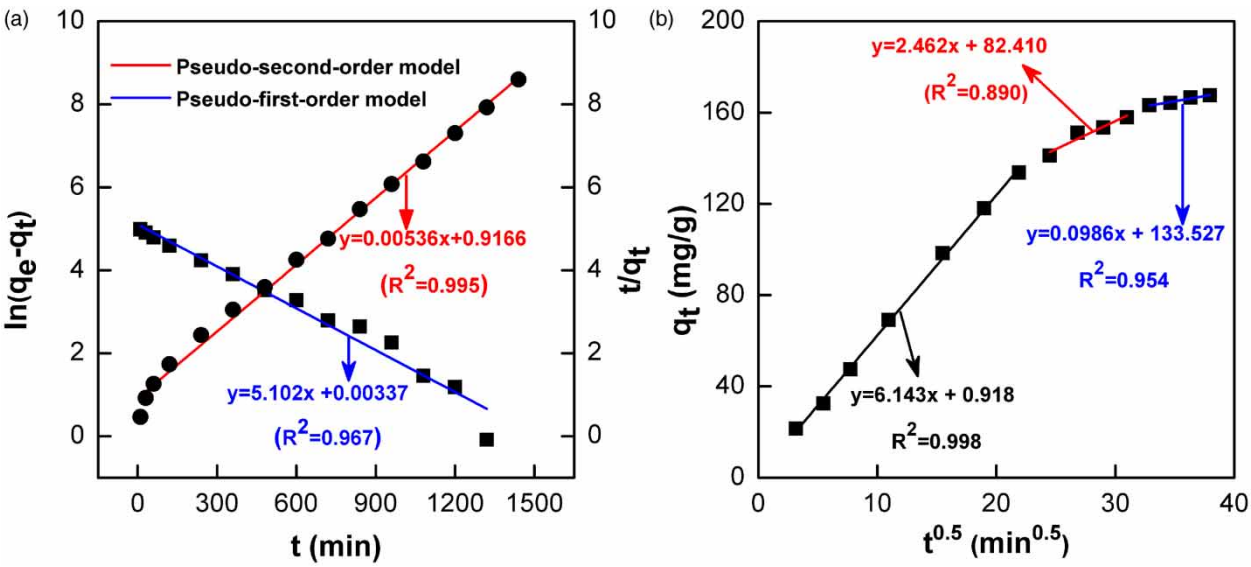

Figure 4 | (a) Pseudo-first-order and pseudo-second kinetic models; (b) intra-particle diffusion model.

the adsorption of Cr(VI) onto AC-TFR-2 compared to the pseudo-first-order equation ($R^2 = 0.967$). This suggests that the removal of Cr(VI) by AC-TFR-2 was mainly controlled by the chemical interactions between the active sites and metal ions (Pang *et al.* 2011).

In addition, the Weber-Morris intra-particle diffusion model (Equation (7)) was also applied for evaluating the adsorption process (Gheju *et al.* 2016).

$$q_t = k_i t^{0.5} + C \tag{7}$$

where q_t (mg/g) denotes the adsorption capacity for Cr(VI) corresponding to time t (min), k_i (mg/g min$^{0.5}$) is the intra-particle diffusion rate constant obtained by calculating the slope of the linear equation of the q_t versus $t^{0.5}$ plot, and C is related to the thickness of the boundary layer.

As shown in Figure 4(b), the plot of q_t versus $t^{0.5}$ had a multilinear character, indicating that three steps of Cr(VI) removal from the solution occurred during the whole process. The intra-particle diffusion constants calculated were $k_1 = 6.143$, $k_2 = 2.462$, and $k_3 = 0.086$, which suggested that the order of the Cr(VI) removal rates was $k_1 > k_2 > k_3$. In the first stage, a higher concentration of Cr(VI) and more active adsorption sites resulted in a high removal rate. With the decrease in Cr(VI) concentration, the number of active adsorption sites decreased in the second stage, thus leading to a decrease in the removal rate. The last stage was the equilibrium state, during which the adsorbed amount of Cr(VI) was nearly unchanged and the removal rate decreased further (Vu *et al.* 2017).

Influence of the initial Cr(VI) concentration and adsorption isotherms

The effect of the initial Cr(VI) concentration on the equilibrium amount of Cr(VI) uptake by AC-TFR-2 was studied, and the result is presented in Figure 3(d). The adsorption capacity of AC-TFR-2 showed a large increase at low Cr(VI) concentrations, while at higher Cr(VI) concentrations, the adsorption capacity increase slowed down. This change from fast to slow was related to the fixed number of active sites. Moreover, the maximum adsorption capacity increased from 140.99 to 172.75 mg/g with the temperature increasing from 288 to 298 K. The increase in adsorption capacity with increasing temperature indicated that the number of adsorption sites increased at higher temperatures, and the adsorbent enabled the transition of the activation energy barrier for uptake (Caner *et al.* 2009).

Two traditional adsorption isotherms, the Langmuir (Equation (8)) and Freundlich (Equation (9)) isotherm models, were used to evaluate the relationship between the amount of Cr(VI) adsorbed onto AC-TFR-2 and its residual in the aqueous solution at equilibrium (Yu *et al.* 2017).

$$\frac{C_e}{q_e} = \frac{C_e}{Q} + \frac{1}{Qb} \tag{8}$$

$$\ln q_e = \ln k_F + \frac{1}{n} \ln C_e \tag{9}$$

where q_e (mg/g) is the amount of Cr(VI) removed by AC-TFR-2 at equilibrium, C_e (mg/L) is the equilibrium residual concentration of Cr(VI) in solution, Q (mg/g) represents the theoretical maximum adsorption capacity of the adsorbate, b (L/mg) is the Langmuir binding constant related to the energy of adsorption, and k_F and n are the capacity factor and the intensity factor of the Freundlich model, respectively. The value of n indicates whether the removal process is favourable ($n > 1$) or unfavourable ($n < 1$).

Moreover, the Langmuir isotherm model can be explained with a dimensionless constant separation factor or equilibrium parameter R_L (Equation (10)) (Pan *et al.* 2016).

$$R_L = \frac{1}{1 + bC_0} \tag{10}$$

where b (L/mg) is the Langmuir constant and C_0 is the initial concentration (mg/L). The value of R_L indicates whether the removal process is favourable ($0 < R_L < 1$) or unfavourable ($R_L > 1$).

Figure 5 shows the Langmuir and Freundlich model plots obtained by fitting the Cr(VI) adsorption data onto AC-TFR-2 at 288, 298 and 308 K. The calculated constants of the two models from the plots are presented in Table 1. The values of the correlation coefficient (R^2) of the Langmuir model at 288, 298 and 308 K were better than those of the Freundlich model, which indicated that the Langmuir model fitted the Cr(VI) adsorption data onto AC-TFR-2 well. In addition, the values of R_L were in the range of 0–1, indicating that the adsorption process was favourable. These results implied monolayer adsorption of Cr(VI) onto AC-TFR-2, and the adsorption process could be carried out again (Gupta *et al.* 2016; Habiba *et al.* 2017a, 2017b). Although the values of the correlation coefficient (R^2) of the Freundlich model were lower than those of the

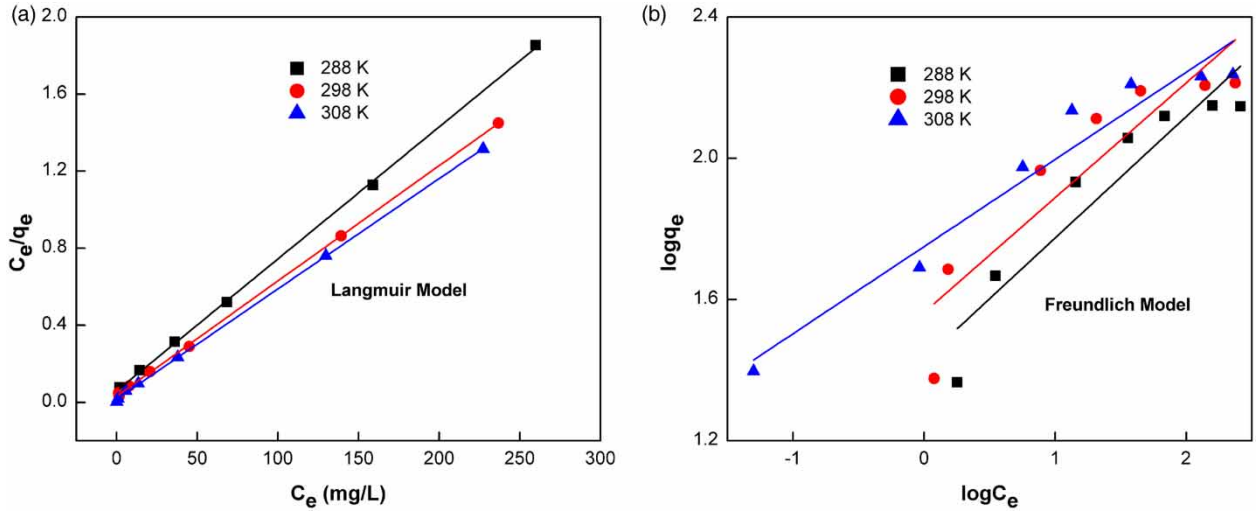

Figure 5 | (a) Langmuir and (b) Freundlich models of Cr(VI) removal.

Table 1 | Langmuir and Freundlich model parameters for Cr(VI) removal by AC-TFR-2

	Langmuir model				Freundlich model		
	Q (mg/g)	b (L/mg)	R_L	R^2	k_F (mg/g) (L/mg)$^{1/n}$	n	R^2
288 K	145.99	0.115	0.021–0.258	0.999	26.98	2.91	0.859
298 K	167.22	0.185	0.013–0.178	0.999	36.43	3.08	0.802
308 K	174.52	0.352	0.007–0.102	0.999	56.23	4.06	0.939

Langmuir model, the Freundlich model could also be used to roughly evaluate the experimental data. The calculated values of n between 2 and 4 suggested the favourable adsorption of Cr(VI) onto AC-TFR-2. The maximum adsorption capacities calculated by the Langmuir model were 145.99 (288 K), 167.22 (298 K) and 174.52 (308 K) mg/g at the different temperatures.

Adsorption thermodynamics

Thermodynamic parameters such as the standard free energy change (ΔG°), standard entropy change (ΔS°) and standard enthalpy change (ΔH°) were estimated at 288, 298 and 308 K to evaluate the feasibility and spontaneity of Cr(VI) adsorption onto AC-TFR-2.

The change in ΔG° can be expressed as Equation (11).

$$\Delta G^\circ = -RT\ln k_c \tag{11}$$

where ΔG° is the standard free energy change (kJ/mol), T (K) is the temperature, R (8.314 J/(mol·K)) is the universal gas constant, and k_c is the adsorption distribution coefficient, which was calculated from the slope of the plot of $\ln(q_e/C_e)$ against C_e at different temperatures and extrapolating to zero C_e (Karthik & Meenakshi 2015).

The relationship of ΔS° and ΔH° of adsorption is described by Equation (12).

$$\ln k_c = \frac{\Delta S^\circ}{R} - \frac{\Delta H^\circ}{RT} \tag{12}$$

where ΔS° is the standard entropy change (kJ/(mol·K)) and ΔH° is the standard enthalpy change (kJ/mol). The values of ΔS° and ΔH° were calculated from the slope and intercept, respectively, of the plot of $\ln k_c$ against $1/T$.

The calculated thermodynamic parameter values for Cr(VI) removal onto AC-TFR-2 are summarized in Table 2. At the different temperatures, the calculated values of ΔG° were negative, which implied the thermodynamic feasibility and spontaneous nature of Cr(VI) adsorption onto AC-TFR-2. In addition, the value of ΔG° decreased with increasing temperature, indicating that adsorption became more

Table 2 | Thermodynamic parameters of Cr(VI) adsorption onto AC-TFR-2

Thermodynamic parameters			
T (K)	ΔG° (kJ/mol)	ΔH° (kJ/mol)	ΔS°(kJ/mol K)
288	−4.94	56.08	0.21
298	−6.49		
308	−9.19		

favourable at higher temperatures. Higher temperatures overcame the activation energy barrier of adsorption and increased the active sites on the surface of AC-TFR-2 (Caner *et al.* 2009). The positive values of ΔH° indicated that adsorption was an endothermic process. ΔH° can offer insight into the type of adsorption process. It has already been reported that the ΔH° values for physical adsorption involving electrostatic adsorption vary between 2.1 and 20.9 kJ/mol, while for chemical adsorption involving complexation, the ΔH° values vary between 20.9 and 418.4 kJ/mol (Kumar *et al.* 2013; Vu *et al.* 2017). In the present work, the ΔH° value of 56.08 kJ/mol was in the range of 20.9–418.4 kJ/mol, the range for the chemical adsorption process. The positive value of ΔS° reflected the increased randomness at the solid-solution interface during Cr(VI) adsorption onto AC-TFR-2.

Influence of coexisting ions

Coexisting cations might exert a negative influence on Cr(VI) removal. Therefore, the effects of several cations on Cr(VI) adsorption, including Na^+, K^+, Ca^{2+}, Mg^{2+} and $Al^{3+,}$ were investigated. The experiments were carried out as binary systems at a fixed Cr(VI) concentration of 200 mg/L and a coexisting cation concentration of 200 mg/L. As shown in Figure 6(a), Cr(VI) removal was unaffected by all the coexisting cations, which could be explained by the fact that the coexisting cations did not participate in the oxidation-reduction reaction and the number of active adsorption sites seemed to remain unchanged.

Reusable performance studies

To investigate the regeneration behaviour of the prepared AC-TFR-2, 0.1 g of AC-TFR-2 previously used for Cr(VI) removal was added to 1 M HCl and stirred well for 120 min. Then, the beads were filtered and washed thoroughly. Thereafter, the ability of AC-TFR-2 to be reused for Cr(VI) adsorption under the same constant parameters was examined. The result is shown in Figure 6(b). The Cr(VI) removal rate gradually decreased from 90.94% to 45.28% at the end of four cycles. This might be ascribed to the decrease in available active sites. Overall, the encapsulation of TFR into AC facilitated the separation and regeneration of the biosorbent.

Adsorption mechanism

To examine the adsorption mechanism of Cr(VI) onto AC-TFR-2, FTIR and XPS were performed to identify the adsorbent before (AC-TFR-2) and after Cr(VI) adsorption

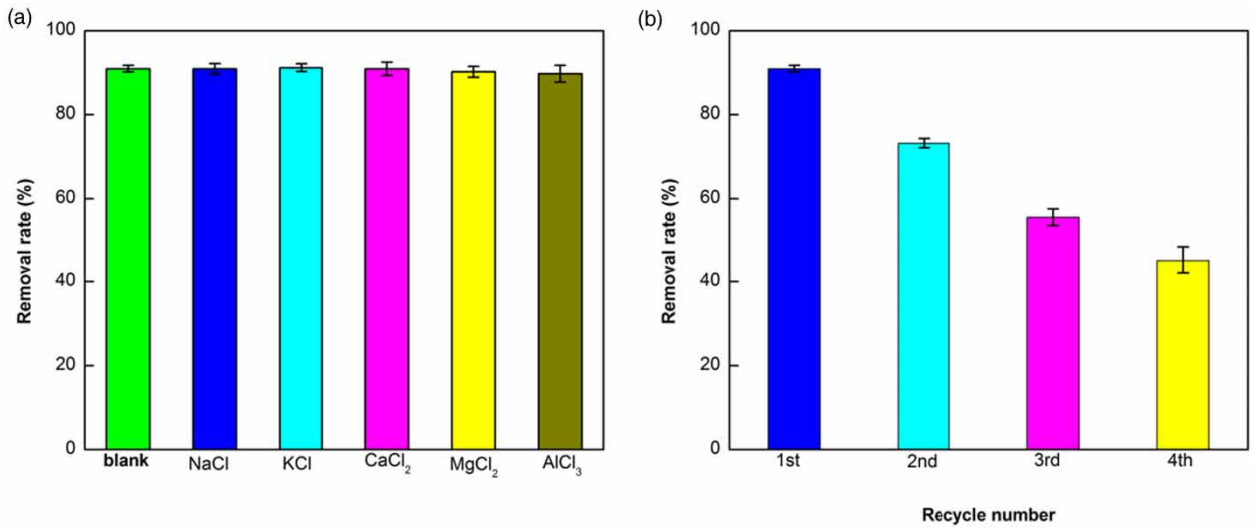

Figure 6 | (a) Effect of coexisting ions on the Cr(VI) removal rate and (b) reusability of AC-TFR-2 for Cr(VI) removal (pH = 2, C_0 = 200 mg/L, V = 100 mL, dosage = 0.1 g, t = 24 hours, and T = 298 K).

(AC-TFR-2-Cr). The FTIR spectrum of AC-TFR-2-Cr is shown in Figure 1(a). Compared with the FTIR spectrum of AC-TFR-2, a new adsorption peak at 1,718.36 cm^{-1} related to the –C = O group appeared, which resulted from the oxidation of TFR by Cr(VI), occurring in parallel to the reduction of Cr(VI) to Cr(III) (Nakano *et al.* 2001). Another change in AC-TFR-2-Cr was the appearance of a sharp and broad peak at 1,384.27 cm^{-1}, which could be attributed to stretching of the carboxylate group (Rodrigues *et al.* 2015). Moreover, a new broad peak at 513.57 cm^{-1} characteristic of Cr-O indicated that Cr was adsorbed onto the AC-TFR-2 framework (Liu *et al.* 2018).

Figure 7(a) shows the representative XPS spectra of AC-TFR-2 and AC-TFR-2-Cr. Mainly C, O, Ca and Na occurred in AC-TFR-2. After adsorption, Cr was also observed, indicating that Cr was adsorbed onto AC-TFR-2, which was consistent with the FTIR results. Simultaneously, Na and Ca disappeared from the XPS spectrum of AC-TFR-2-Cr, which could be ascribed to ion exchange with hydrogen and chromium ions. In Figure 7(b), the Cr high-resolution XPS signal was curve-fitted to two peaks, corresponding to Cr 2 p1/2 and Cr 2 p3/2. The binding energies of the two peaks were at 586.48 and 577.23 eV, respectively, which are characteristic of Cr(III) (Liu *et al.* 2018). This result confirmed that Cr(VI) was reduced to Cr(III) during the adsorption process. Figure 7(c) and 7(d) show the C 1s high-resolution XPS spectra of AC-TFR-2 and AC-TFR-2-Cr, respectively. Before Cr(VI) adsorption, the C 1s XPS spectra of AC-TFR-2 were fitted to three peaks of C-C (284.14 eV), C–O (285.82 eV) and C = O (288.05 eV). After Cr(VI) adsorption, the binding energies of the corresponding peaks increased to 284.31, 286.10 and 288.24 eV, respectively. The change in C 1s binding energy indicated that carbon atoms in AC-TFR-2 were involved in Cr(VI) uptake (Xia *et al.* 2018). This result can likely be explained by Cr(III) replacing calcium ions on AC-TFR-2. Cr(III) possessed more positive charges than dicalcium, which resulted in an increase in the C 1s binding energy.

Based on the results mentioned above, the presumed adsorption mechanism of Cr(VI) onto AC-TFR-2 is

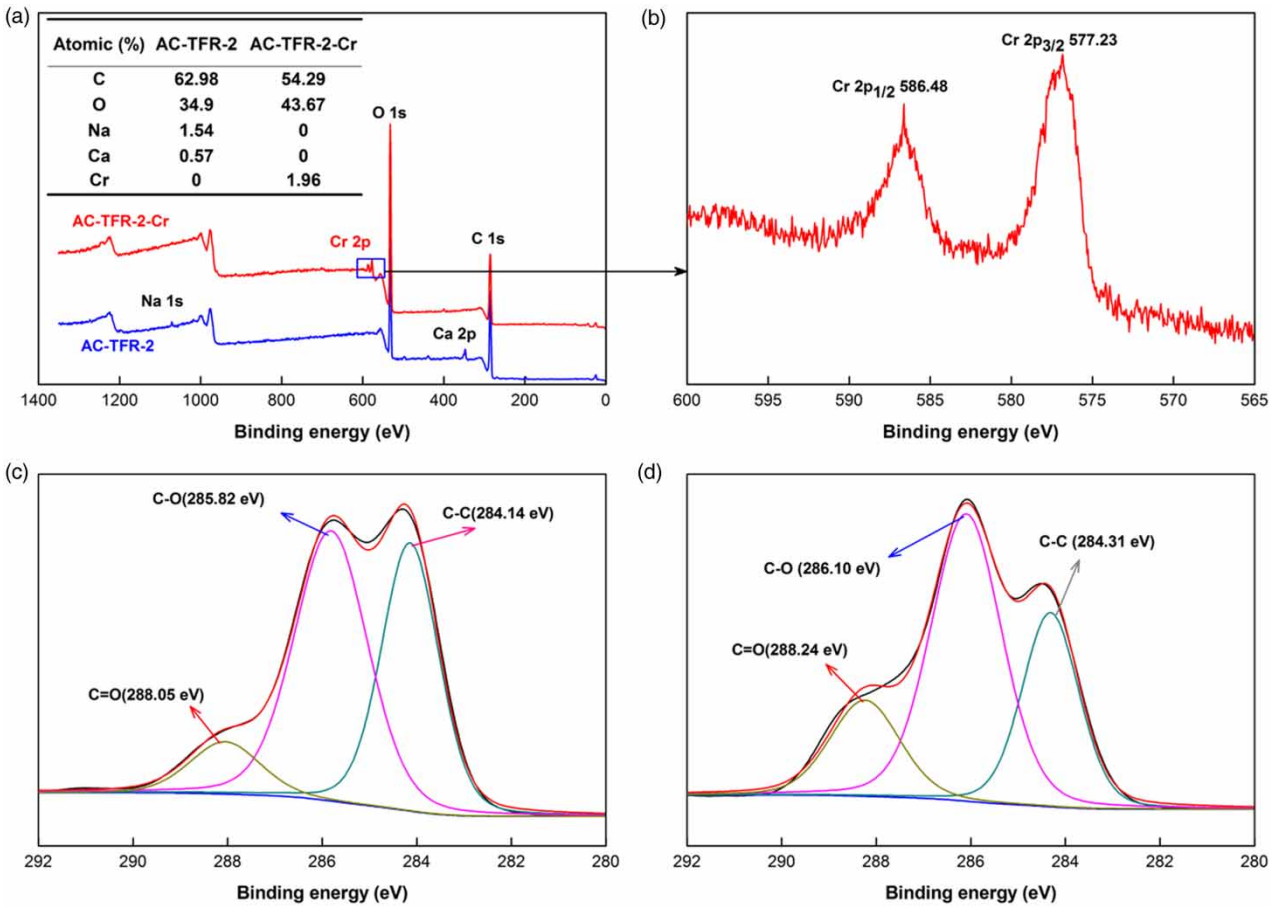

Figure 7 | (a) XPS spectra of AC-TFR-2 and AC-TFR-2-Cr; (b) Cr 2p high-resolution XPS spectrum; and C 1 s high-resolution XPS spectra of (c) AC-TFR-2 and (d) AC-TFR-2-Cr.

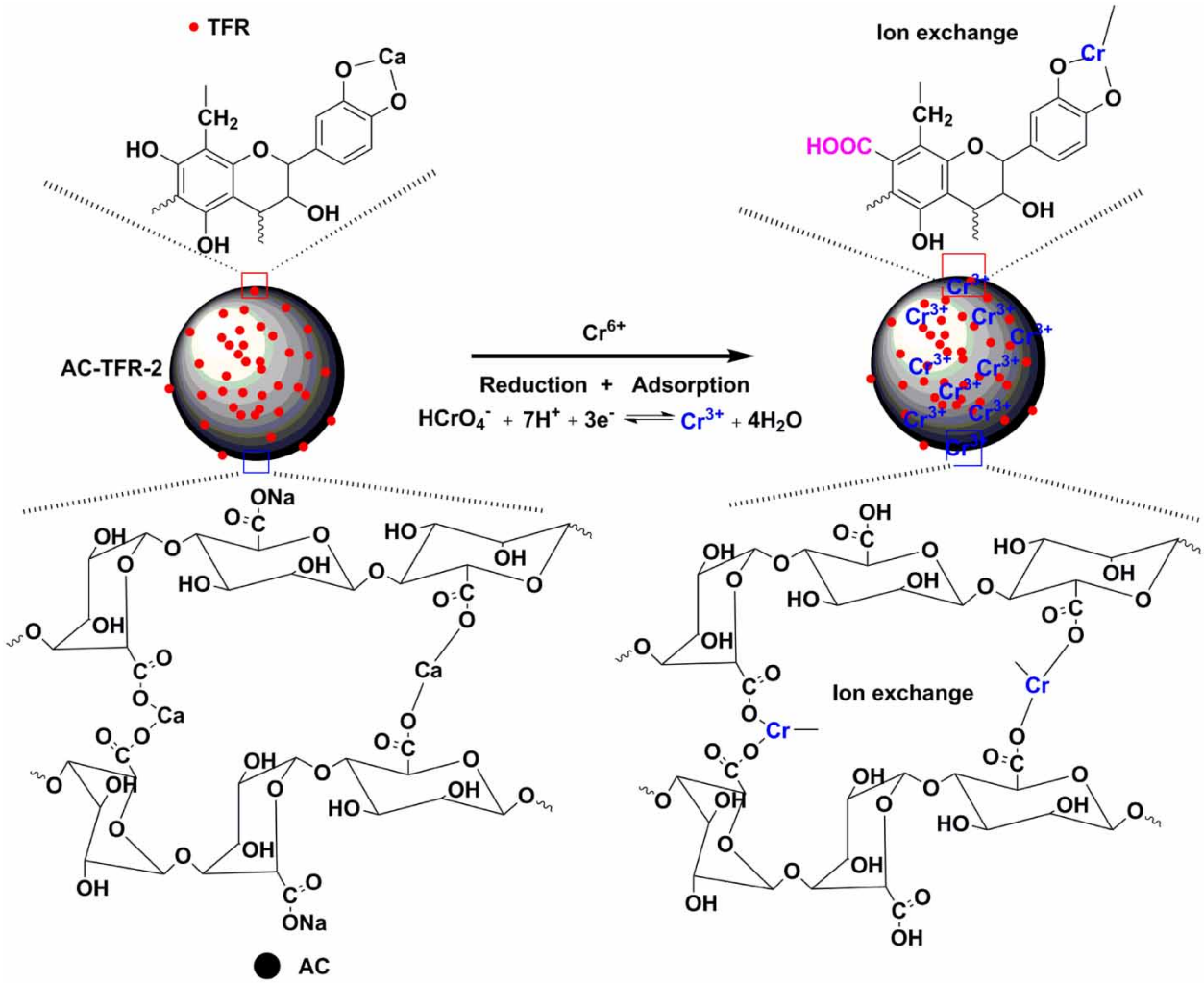

Figure 8 | Schematic illustration of the reduction-adsorption mechanism of Cr(VI) onto AC-TFR-2.

schematically shown in Figure 8. First, Cr(VI) was reduced to Cr(III) by the hydroxyphenyl groups of TFR, which were oxidized to form carboxyl groups. Then, Cr(III) chelated onto AC-TFR-2 through ion exchange with calcium ions.

CONCLUSION

Tannin-based biosorbent (AC-TFR) was successfully prepared by impregnating tannin-formaldehyde resin (TFR) into calcium alginate beads (AC) and applied in Cr(VI) removal from an aqueous solution. Under the experimental conditions, AC-TFR-2 (mass ratio of AC: TFR = 1:1) showed an excellent adsorption capacity compared with the other AC-TFR adsorbents. Cr(VI) removal by AC-TFR-2 was significantly influenced by pH. The calculated adsorption parameters revealed that the adsorption process obeyed the pseudo-second-order kinetic and Langmuir models and was subject to a rate-controlling step. The maximum adsorption capacities of AC-TFR-2 evaluated by the Langmuir model were 145.99, 167.22 and 174.52 mg/g at 288, 298, and 308 K, respectively. The calculated values of the thermodynamic parameters for Cr(VI) removal by AC-TFR-2 indicated that the adsorption process was endothermic and spontaneous in nature and relied on chemical adsorption. The Fourier transform infrared spectroscopy (FTIR), X-ray diffraction (XRD) and scanning electron microscopy (SEM) results showed that TFR was successfully impregnated into AC. The X-ray photoelectron spectroscopy (XPS) and FTIR spectra indicated that Cr was successfully adsorbed onto AC-TFR-2 and that the mechanism of Cr(VI) removal was mainly driven by reduction and ion

exchange. Impregnating TFR into AC not only improved the adsorption capacity of AC for Cr(VI) but also facilitated the separation of TFR. Briefly, AC-TFR can be applied as a promising potential and sustainable adsorbent for Cr(VI) removal in aqueous solutions.

ACKNOWLEDGEMENTS

This work was financially supported by the Scientific & Technology of Sichuan Province (2019YJ0399).

REFERENCES

Aharchaou, I., Py, J.-S., Cambier, S., Loizeau, J.-L., Cornelis, G., Rousselle, P., Battaglia, E. & Vignati, D. A. L. 2018 Chromium hazard and risk assessment: new insights from a detailed speciation study in a standard test medium. *Environ. Toxicol. Chem.* **37**, 983–992.

Arbenz, A. & Avérous, L. 2015 Chemical modification of tannins to elaborate aromatic biobased macromolecular architectures. *Green Chem.* **46**, 2626–2646.

Bacelo, H. A. M., Santos, S. C. R. & Botelho, C. M. S. 2016 Tannin-based biosorbents for environmental applications – A review. *Chem. Eng. J.* **303**, 575–587.

Bertagnolli, G., Grishin, A., Vincent, T. & Guibal, E. 2015 Synthesis and application of a novel sorbent (tannic acid-grafted-polyethyleneimine encapsulated in alginate beads) for heavy metal removal. *Sep. Sci. Technol.* **50**, 2897–2906.

Caner, N., Kiran, I. & Ilhan, S. 2009 Isotherm and kinetic studies of Burazol Blue ED dye biosorption by dried anaerobic sludge. *J. Hazard. Mater.* **165**, 279–284.

Chand, R., Narimura, K., Kawakita, H., Ohto, K., Watari, T. & Inoue, K. 2009 Grape waste as a biosorbent for removing Cr(VI) from aqueous solution. *J. Hazard. Mater.* **163**, 245–250.

Chang, X., Li, M., Liu, Q., Liu, Q. & Yao, J. 2016 Adsorption-reduction of chromium(VI) from aqueous solution by phenol-formaldehyde resin microspheres. *RSC Adv.* **6**, 46879–46888.

Doan, V. D., Le, V. T., Le, H. S., Ta, D. H. & Nguyen, H. T. 2019 Effectiveness of calcium deficiency in nanosized hydroxyapatite for removal of Fe(II), Cu(II), Ni(II) and Cr(VI) ions from aqueous solutions. *J. Nano. Res-SW.* **56**, 17–27.

Fiol, N., Poch, J. & Villaescusa, I. 2005 Grape stalks wastes encapsulated in calcium alginate beads for Cr(VI) removal from aqueous solutions. *Sep. Sci. Technol.* **40**, 1013–1028.

Gheju, M., Balcu, I. & Mosoarca, G. 2016 Removal of Cr(VI) from aqueous solutions by adsorption on MnO_2. *J. Hazard. Mater.* **310**, 270–277.

Googerdchian, F., Moheb, A. & Emadi, R. 2012 Lead sorption properties of nanohydroxyapatite–alginate composite adsorbents. *Chem. Eng. J.* **200–202**, 471–479.

Gopalakannan, V. & Viswanathan, N. 2016 One pot synthesis of metal ion anchored alginate–gelatin binary biocomposite for efficient Cr(VI) removal. *Int. J. Biol. Macromol.* **83**, 450–459.

Gupta, V. K., Chandra, R., Tyagi, I. & Verma, M. 2016 Removal of hexavalent chromium ions using CuO nanoparticles for water purification applications. *J. Colloid Interf. Sci.* **478**, 54–62.

Gurung, M., Adhikari, B. B., Kawakita, H., Ohto, K., Inoue, K. & Alam, S. 2011 Recovery of Au(III) by using low cost adsorbent prepared from persimmon tannin extract. *Chem. Eng. J.* **174**, 556–563.

Habiba, U., Afifi, A. M., Salleh, A. & Ang, B. C. 2017a Chitosan/(polyvinyl alcohol)/zeolite electrospun composite nanofibrous membrane for adsorption of Cr^{6+}, Fe^{3+} and Ni^{2+}. *J. Hazard. Mater.* **322**, 182–194.

Habiba, U., Siddique, T. A., Joo, T. C., Salleh, A., Ang, B. C. & Afifi, A. M. 2017b Synthesis of chitosan/polyvinyl alcohol/zeolite composite for removal of methyl orange, Congo red and chromium(VI) by flocculation/adsorption. *Carbohyd. Polym.* **157**, 1568–1576.

Han, Y., Cao, X., Ouyang, X., Sohi, P. & Chen, J. 2016 Adsorption kinetics of magnetic biochar derived from peanut hull on removal of Cr(VI) from aqueous solution: effects of production conditions and particle size. *Chemosphere* **145**, 336–341.

Hokkanen, S., Bhatnagar, A., Repo, E., Lou, S. & Sillanpaa, M. 2016 Calcium hydroxyapatite microfibrillated cellulose composite as a potential adsorbent for the removal of Cr(VI) from aqueous solution. *Chem. Eng. J.* **283**, 445–452.

Ibáñez, J. P. & Umetsu, Y. 2002 Potential of protonated alginate beads for heavy metals uptake. *Hydrometallurgy* **64**, 89–99.

Kamel, M. M., EI-Mgeed, A. M. A. & EI-Hewaihy, M. A. I. 2013 Synthesis of a novel tannin-formaldehyde resin from *Acacia nilotica* fruit extract and its viability for adsorption of manganese form ground water. *Water Sci. Technol.* **13**, 1236–1248.

Karthik, R. & Meenakshi, S. 2015 Removal of Cr(VI) ions by adsorption onto sodium alginate-polyaniline nanofibers. *Int. J. Biol. Macromol.* **72**, 711–717.

Kumar, R., Ansari, M. O. & Barakat, M. A. 2013 DBSA doped polyaniline/multi walled carbon nanotubes composite for high efficiency removal of Cr(VI) from aqueous solution. *Chem. Eng. J.* **228**, 748–755.

Kumar, R., Kim, S., Kim, K., Lee, S., Park, H. & Jeon, B. 2017 Removal of hazardous hexavalent chromium from aqueous phase using zirconium oxide-immobilized alginate beads. *Appl. Geochem.* **88**, 113–121.

Lazaridis, N. K. & Charalambous, C. 2005 Sorptive removal of trivalent and hexavalent chromium from binary aqueous solutions by composite alginate-geothite beads. *Water Res.* **39**, 4385–4396.

Lee, C. G., Park, J. A., Lee, I., Kang, J. K., Yoon, S. Y. & Kim, S. G. 2013 Preparation of magnetic alginate–layered double hydroxide composite adsorbents and removal of Cr(VI) from aqueous solution. *Water Sci. Technol.-Water Supply* **13**, 846–853.

Liu, Q., Liu, Q., Liu, B., Hu, B., Hu, T., Liu, W. & Yao, J. 2018 Green synthesis of tannin-hexamethylendiamine based

adsorbents for efficient removal of Cr(VI). *J. Hazard. Mater.* **352**, 27–35.

Nakajima, A. & Baba, Y. 2004 Mechanism of hexavalent chromium adsorption by persimmon tannin gel. *Water Res.* **38**, 2859–2864.

Nakano, Y., Takeshita, K. & Tsutsumi, T. 2001 Adsorption mechanism of hexavalent chromium by redox within condensed-tannin gel. *Water Res.* **35**, 496–500.

Nasrullah, A., Bhat, A. H., Naeem, A., Isa, M. H. & Danish, M. 2017 High surface area mesoporous activated carbon-alginate beads for efficient removal of methylene blue. *Int. J. Biol. Macromol.* **107**, 1792–1799.

Özacar, M., Şengil, İ. A. & Türkmenler, H. 2008 Equilibrium and kinetic data, and adsorption mechanism for adsorption of lead onto valonia tannin resin. *Chem. Eng. J.* **143**, 32–42.

Pan, Y., Cai, P., Farmahini-Farahani, M., Li, Y., Hou, X. & Xiao, H. 2016 Aminofunctionalized alkaline clay with cationic star-shaped polymer as adsorbents for removal of Cr(VI) in aqueous solution. *Appl. Surf. Sci.* **385**, 333–340.

Pang, Y., Zeng, G. M., Tang, L., Zhang, Y., Liu, Y. Y., Lei, X. X., Li, Z., Zhang, J. H., Liu, Z. C., Liu, Z. F. & Xiong, Y. Q. 2011 Preparation and application of stability enhanced magnetic nanoparticles for rapid removal of Cr(VI). *Chem. Eng. J.* **175**, 222–227.

Peretz, S., Anghel, D. F., Vasilescu, E., Florea-Spiroiu, M., Stoian, C. & Zgherea, G. 2015 Synthesis, characterization and adsorption properties of alginate porous beads. *Polym. Bull.* **72**, 3169–3182.

Rahman, M. M., Akter, N., Karim, M. R., Ahmad, N., Rahman, M. M., Siddiquey, I. A., Bahadur, N. M. & Hasnat, M. A. 2014 Optimization, kinetic and thermodynamic studies for removal of Brilliant Red (X-3B) using tannin gel. *J. Environ. Chem. Eng.* **2**, 76–83.

Ren, X., Chen, C., Nagatsu, M. & Wang, X. 2011 Carbon nanotubes as adsorbents in environmental pollution management: a review. *Chem. Eng. J.* **170**, 395–410.

Rodrigues, L. A., Sakane, K. K., Simonetti, E. A. N. & Thim, G. P. 2015 Cr total removal in aqueous solution by PHENOTAN AP based tannin gel (TFC). *J. Environ. Chem. Eng.* **3**, 725–733.

Sánchez-Martín, J., González-Velasco, M., Beltrán-Heredia, J., Gragera-Carvajal, J. & Salguero-Fernández, J. 2010 Novel tannin-based adsorbent in removing cationic dye (Methylene Blue) from aqueous solution: kinetics and equilibrium studies. *J. Hazard. Mater.* **174**, 9–16.

Şengil, İ. A. & Özacarb, M. 2008 Biosorption of Cu(II) from aqueous solutions by mimosa tannin gel. *J. Hazard. Mater.* **157**, 277–285.

Sillerová, H., Komárek, M., Liu, C., Poch, J. & Villaescusa, I. 2015 Biosorbent encapsulation in calcium alginate: effects of process variables on Cr(VI) removal from solutions. *Int. J. Biol. Macromol.* **80**, 260–270.

Suganya, S. & Kumar, P. S. 2018 Influence of ultrasonic waves on preparation of active carbon from coffee waste for the reclamation of effluents containing Cr(VI) ions. *J. Ind. Eng. Chem.* **60**, 418–430.

Vu, H. C., Dwivedi, A. D., Le, T. T., Seo, S., Kim, H. E. J. & Chang, Y. S. 2017 Magnetite graphene oxide encapsulated in alginate beads for enhanced adsorption of Cr(VI) and As(V) from aqueous solutions: role of crosslinking metal cations in pH control. *Chem. Eng. J.* **307**, 220–229.

Wang, X., Wen, T., Tan, X., Chen, Y., Chen, C., Xu, A. W. & Fan, Q. 2016 A core–shell structure of polyaniline coated protonic titanate nanobelt composites for both Cr(VI) and humic acid removal. *Polym. Chem-UK.* **7**, 785–794.

Wang, D., Zhang, G., Zhou, L., Wang, M., Cai, D. & Wu, Z. 2017 Synthesis of a multifunctional graphene oxide-Based magnetic nanocomposite for efficient removal of Cr(VI). *Langmuir* **33**, 7007–7014.

Wu, J., Wang, X. B. & Zeng, R. J. 2017 Reactivity enhancement of iron sulfide nanoparticles stabilized by sodium alginate: taking Cr (VI) removal as an example. *J. Hazard. Mater.* **333**, 275–284.

Xia, M., Zheng, X. M., Du, M. Y., Wang, Y. Y., Ding, A. Z. & Dou, J. F. 2018 The adsorption of Cs^{+} from wastewater using Lithium-modified montmorillonite caged in calcium alginate beads. *Chemosphere* **203**, 271–280.

Xu, M. H., Cao, F., Tang, P. S. & Wang, K. Y. 2013 Preparation of calcium alginate metal ion gel beads and its adsorption of $Cr_2O_7^{2-}$. *Materials Review* **27**, 78–83.

Yu, R., Shi, Y., Yang, D., Liu, Y., Qu, J. & Yu, Z. Z. 2017 Graphene oxide/chitosan aerogel microspheres with honeycomb-cobweb and radially oriented microchannel structures for broad-spectrum and rapid adsorption of water contaminants. *ACS Appl. Mater. Inter.* **9**, 21809–21819.

Zhao, Y., Qi, W., Chen, G., Ji, M. & Zhang, Z. 2015 Behavior of Cr(VI) removal from wastewater by adsorption onto HCl activated Akadama clay. *J. Taiwan Inst. Chem.* **50**, 190–197.

First received 9 January 2020; accepted in revised form 3 April 2020. Available online 16 April 2020